REGULAR ARTICLE

Phenomenological description of the transition state, and the bond breaking and bond forming processes of selected elementary chemical reactions: an information-theoretic study

Rodolfo O. Esquivel · Nelson Flores-Gallegos · Cristina Iuga · Edmundo M. Carrera · Juan Carlos Angulo · Juan Antolín

Abstract Theoretic-information measures of the Shannon type are employed to describe the course of the simplest hydrogen abstraction and the identity S_N2 exchange chemical reactions. For these elementary chemical processes, the transition state is detected and the bond breaking/forming regions are revealed. A plausibility argument of the former is provided and verified numerically. It is shown that the information entropy profiles posses much more chemically meaningful structure than the profile of the total energy for these chemical reactions. Our results support the concept of a continuum of transient of Zewail and Polanyi for the transition state rather than a single state, which is also in agreement with reaction force analyses. This is performed by following the intrinsic reaction coordinate (IRC) path calculated at the MP2 level of theory from which Shannon entropies in position and momentum spaces at the QCISD(T)/6-311++G(3df,2p) level are determined. Several selected descriptors of the density are utilized to support the observations, such as the molecular electrostatic potential, the hardness, the dipole moment along with geometrical parameters.

1 Introduction

The prediction, from first principles, of the structure and energetics of molecules when exerting physical changes, such as dissociations or chemical reactions, constitutes a major activity of theoretical/computational chemistry. Such an endeavor has not been an easy one though, involving several research areas which have provided solid grounds and fertile soil for theories and models that have pervaded over the years in ongoing research efforts that have been thoroughly discussed in the literature [1]. We will review here some of the conditions that have brought up the need of characterizing chemical processes in terms of physical phenomena, such as charge depletion/accumulation, bond breaking/forming, path reaction-following etc.

In an attempt to understand the stereochemical course of chemical reactions, calculations of potential energy surfaces have been carried out extensively at various levels of sophistication [2]. Within the broad scope of these investigations, particular interest has been focused on extracting information about the stationary points of the energy surface. Considering the Born–Oppenheimer approximation, minima on the N-dimensional potential energy surface for the nuclei can be identified with the classical picture of equilibrium structures of molecules and saddle points can be related to transition states and reaction rates. Since the formulation of transition-state (TS) theory [3, 4], a great effort has been devoted to developing models for

R. O. Esquivel (✉) · N. Flores-Gallegos · C. Iuga · E. M. Carrera
Departamento de Química, Universidad Autónoma
Metropolitana, 09340 Mexico D.F., Mexico
e-mail: esquivel@xanum.uam.mx; esqol@ugr.es

R. O. Esquivel · J. C. Angulo
Departamento de Física Atómica, Molecular y Nuclear,
Universidad de Granada, 18071 Granada, Spain

R. O. Esquivel · J. C. Angulo · J. Antolín
Instituto Carlos I de Física Teórica y Computacional,
Universidad de Granada, 18071 Granada, Spain

J. Antolín
Departamento de Física Aplicada, EUITIZ,
Universidad de Zaragoza, 50018 Zaragoza, Spain

characterizing the TS, which is assumed to govern the height of a chemical reaction barrier, so that any insights into the nature of the TS are likely to provide deeper understanding of the chemical reactivity. Computational quantum chemistry has sidestepped the inherent problems by managing rigorous mathematical definitions of "critical points" on a potential energy hypersurface, and thence assigned to equilibrium complexes or transition states. Within this approach, minima and saddle points have been fully characterized through the first and second derivatives of the energy (gradient and Hessian) over the nuclei positions. That is, if there is more than one minimum on a contiguous energy surface, a family of paths can be obtained that connect one minimum to the other and if the highest energy point on each path is considered, the TS can be defined then as the lowest of these maxima along the reaction path, and a minimum for all displacements perpendicular to that path, i.e., a first-order saddle point. The eigenvector corresponding to the single negative eigenvalue of this critical point is the transition vector. It is so that the steepest-descent path from the saddle point to either of the two minima (reactants or products) follows this vector. Since the minima and the transition state are well-defined points on the energy surface, it is possible to define a unique reaction path, though it would depend on the particular choice of the coordinate system. This problem was solved by defining an intrinsic reaction path independent of the coordinate system by appealing to classical mechanics in which the motion equations are the simplest in mass-weighted Cartesian coordinates [5]. Then an intrinsic reaction coordinate (IRC) can be defined as the path traced by a classical particle moving with infinitesimal velocity from a saddle point down to the minima and the IRC is unique in virtue of the classical equations of motion which should be the same in any coordinate system. In mass-weighted coordinates the IRC and the steepest-descent path are the same. Several computational techniques which calculate energy gradients and Hessians have been developed to follow such reaction paths [6–15].

Notwithstanding that critical points of the energy surface are useful mathematical features for analyzing the reaction-path, their chemical and physical meaning remains uncertain [16]. Chemical concepts, such as the reaction rate and the reaction barrier have been thoroughly studied and yet, the pursuit for understanding the TS structure represents a challenge of physical organic chemistry. The many efforts to achieve the latter have produced chemically useful descriptions of the TS, such as the one provided by Hammond and Leffler [17, 18]. Hammond postulated that two points on a reaction profile that are of similar energy will also be of similar structure. This allowed predictions regarding the structure of the transition state to be made in highly exothermic and endothermic reactions. Leffler generalized the idea to the entire range of reaction exothermicities by considering the TS as a hybrid of reactants and products, the character of which is intermediate between these two extremes. These ideas remain as a very practical tool for analyzing chemical reactions now referred to as the Hammond–Leffler postulate which generally states that the properties of the TS are intermediate between reactant and product and are related to the position of the TS along the reaction coordinate.

In the search for providing with a more intuitive quantum chemical basis of the mathematical saddle point (TS), Shaik [19] developed a general model for the TS of a chemical reaction based on the valence-bond theory (VB) through the avoided crossing state (ACS) or the perfectly resonating state (PRS) of the VB configurations that describe a chemical transformation [20, 21]. The PRS is typified by a pairwise resonance (or avoided crossing) between two of the principal valence bond structures which describe the electronic structure of the reaction complexes which intend to describe the TS. While it is true that this approach provides a significantly less rigorous description of the TS, it does enable predictions about TS structure and chemical reactivity to be made. The advantage resides in that the ACS possesses a wave function that is prescribed by the PRS and it is explicit in terms of the participating VB configurations to approximate the TS. The model of Shaik et al. [22–25] has been applied to many areas of chemistry to explain reaction barriers and chemical reactivity. Considering that the TS is a species which varies, geometrically and electronically, in a continuous manner among the well-defined structures of reactants, products, and potential intermediates, it would then be important to obtain more chemically meaningful information about the process in the vicinity of the TS, where the ion-complex species involved in the chemical reaction exert physically important phenomena, such as bond breaking/forming and/or charge depletion/accumulation. This information would be of great value too in assessing whether the ACS/PRS is located on the reaction profile which descends from the saddle point along the reaction vector and in assisting in the locating/designing of PRSs which may enable to trace on the pathways of the chemically meaningful potential hypersurface.

Notwithstanding the apparent success of the ACS–VB model, for some nucleophilic addition reactions of the S_N2 type wherein Hammond–Leffler effects are more pronounced, the TSs exhibit charge distribution patterns which suggest a significant dissimilarity between the TSs and the ACSs [26]. It has been argued [27] that, for these type of nucleophilic reactions, the correlation between the energy barriers and the TS depends on two reactivity features: high energy barriers associated with TSs which are close to their dissociation limits (stretching or "looseness" of the bond

being broken), and on the deformations that are required to carry the ground-state molecules to the TS which affect the reaction barriers, i.e., looseness depends on bond distortion effects dominated by the height of the barriers and on the electron density depletion effects which are dominated by the stability of the ions. Since the representation of the VB diagram focusses on the 'active bonds', those that are being broken or made during the reaction, it would be relevant to have more information in those specific regions, where the molecular density suffers accumulation/depletion effects and bond is breaking/forming, regions which are not specifically provided by the stationary points of the energy hypersurface.

Moreover, the ab initio G2 results of Glukhovtsev et al. [28, 29] for identity and non-identity S_N2 reactions have found their data to be in agreement with the Leffler–Hammond postulate in that there is a correlation between the geometrical asymmetry of the transition state and the reaction exothermicity. This has also been found earlier by Wolfe et al. [30]. On the other hand, Glukhovtsev et al. found excellent correlation between the charge asymmetry ($Q_X - Q_Y$, where Q is the MP2 natural charge either for X or Y) and the geometrical asymmetry [28]. Whether there also is a correlation between the degree of charge development on the nucleophile/nucleofuge (entering/leaving species), and reaction exothermicity or geometrical transition state asymmetry has been the subject of some controversy in the literature. Shaik et al. [30] have suggested that the ACS/PRS is characterized by having equal weights of the reactant and product ion-complex structures. This model was criticized by Shi and Boyd [31] on the grounds that the entering and leaving groups have identical charges in the ACS/PRS for any exothermicity of the reaction, and it was argued that this was at odds with the Leffler–Hammond postulate prediction of early/late transition states being reactant/product-like. However, Shaik et al. [32–35] have shown that the ACS/PRS and transition state lie very close both geometrically as well as energetically, and have argued that there is no necessarily simple linkage between transition state geometry and charge. It appears that further investigations are necessary in order to clarify this issue, and once again the necessity of having more information about the charge development and the earliness/lateness of the transition structure is evident in order to estimate any possible correlations.

With the advent of femtosecond time-resolved methods the aforementioned theories have turned out to be more relevant at the present time. Since the seminal studies of Zewail et al. [36, 37], femto-chemistry techniques have been applied to chemical reactions ranging in complexity from bond-breaking in diatomic molecules to dynamics in larger organic and biological molecules, providing new insights into the understanding of fundamental chemical

processes, on Zewail's words: "chemistry on the femtosecond time scale, can be defined as the field of chemical dynamics concerned with the very act of breaking or making a chemical bond. On this time scale the molecular dynamics are "frozen out", and thus one should be able to observe the complete evolution of the chemical event, starting from time zero, passing through transition states, and ultimately forming products". Although most femtochemistry studies deal with excited-state processes, ground-state processes have been studied as well. One of the most promising techniques, the anion photodetachment spectra [38], has made possible the direct observation of transition states. The femto-time scale is perhaps the ultimate frontier as far as chemistry is concerned, experiments at this level being ultimately limited by the fundamental laws of quantum mechanics through the Heisenberg principle. In order to explain the experimental results of the femto-techniques it will be necessary to complement the existing chemical reactivity theories with electronic density descriptors of the events taking place in the vicinity of the transition-state region, where the chemical bonds are actually being formed or destroyed.

In connection with the above, there are a number of studies in the literature which have employed a variety of descriptors to study either the TS structure or to follow the course of the chemical reaction path. For instance, Shi and Boyd [39] performed a systematic analysis of model S_N2 reactions in order to study the TS charge distribution in connection with the Hammond–Leffler postulate. Bader et al. developed a theory of reactivity based solely on the properties of the charge density by employing the properties of the Laplacian of the density so as to align the local charge concentrations with regions of charge depletion of the reactants. This was achieved by mixing in the lowest energy excited state of the combined system to produce a relaxed charge distribution corresponding to the transition density [40]. By studying the time evolution of a bimolecular exchange reaction Balakrishnan et al. [41] showed that information-theoretic entropies in dual or phase space rose to a maximum in a dynamical study. Following the course of two elementary S_N2 reactions, Ho et al. [42] showed that theoretic-information measures were able to reveal geometrical changes of the density which were not present in the energy profile, although the transition states were not apparent from the study. In an attempt to build a density-based theory of chemical reactivity, Knoerr et al. [43] reported correlations between features of the quantum mechanically determined charge density and the energy-based measures of Shaik et al. [44] to describe the charge transfer, stability and charge localization accompanying an S_N2 reaction. Moreover, Tachibana [45] was able to visualize the formation of a chemical bond of selected model reactions by using the kinetic energy density $n_T(r)$ to

identify the intrinsic shape of the reactants, the TS and the reaction products along the course of the IRC, hence realizing Coulson's conjecture [46] in that the physical meaning of the probability density might be related with the energy density. The reaction force of a system's potential energy along the reaction coordinate has been employed to characterize changes in the structural and/or electronic properties in chemical reactions [47–50]. The Kullback–Leibler information deficiency has been evaluated along molecular internal rotational or vibrational coordinates and along the intrinsic reaction coordinate for several S_N2 reactions [51].

Notwithstanding that there has been a great interest in the last 20 years in applying information theory (IT) measures to the electronic structure of atoms and molecules [52–73], it has not been clearly assessed whether theoretic-information measures are good descriptors for characterizing chemical reaction parameters, i.e., the stationary points of the IRC path (the TS and the equilibrium geometries of the complex species) and the bond breaking/forming regions. The purpose of the present study is to perform a phenomenological description of two selected elementary chemical reactions by following their IRC paths with the purpose of analyzing the behavior of the densities in position and momentum spaces at the vicinity of the TS and also at the regions of bond forming/breaking that are not visible in the energy profile by use of the Shannon entropies in conjugated spaces. In order to witness the density changes exerted by the molecular structures and link them with the theoretic-information quantities during the chemical processes, we will employ several charge density descriptors, such as the molecular electrostatic potential (MEP) and some reactivity parameters of density functional theory (DFT), the hardness and the softness. The chemical probes under study are the simplest hydrogen abstraction reaction $H \cdot + H_2 \rightarrow H_2 + H \cdot$ and the identity S_N2 reaction $H^- + CH_4 \rightarrow CH_4 + H^-$.

2 Theoretical methods

The central quantities under study are the Shannon entropies in position and momentum spaces [74]:

$$S_r = -\int \rho(\mathbf{r}) \ln \rho(\mathbf{r}) d^3\mathbf{r} \qquad (1)$$

$$S_p = -\int \gamma(\mathbf{p}) \ln \gamma(\mathbf{p}) d^3\mathbf{p} \qquad (2)$$

where $\rho(\mathbf{r})$ and $\gamma(\mathbf{p})$ denote the molecular electron density distributions in the position and momentum spaces, respectively, each normalized to unity. The Shannon

entropy in position space S_r constitutes a measure of delocalization or lack of structure of the electronic density in the position space and hence S_r is maximal when knowledge of $\rho(\mathbf{r})$ is minimal and becomes delocalized. The Shannon entropy in momentum space S_p is largest for systems with electrons of higher speed (delocalized $\gamma(\mathbf{p})$) and is smaller for relaxed systems, where kinetic energy is low. Entropy in momentum space S_p is closely related to S_r by the uncertainty relation of Bialynicki-Birula and Mycielski [75], which shows that the entropy sum $S_T = S_r + S_p$, is a balanced measure and cannot decrease arbitrarily. For one-electron atomic systems it may be interpreted as that localization of the electron's position results in an increase of the kinetic energy and a delocalization of the momentum density, and conversely.

In connection with the behavior of the Shannon entropies discussed above, we expect a simple theoretic-information description of the TS in terms of localized/delocalized distributions. Considering that there is no variational principle for any quantum–mechanical property other than the energy, deriving a direct relation between the TS and the Shannon entropies as functionals of the electron densities seems not practical and surely beyond the scope of the present work. Instead, we present with a plausible physical argument to link both quantities: on mathematical grounds the TS represents a first-order saddle point connecting two minima in a topological sense, and physically it represents a maximum in the "potential energy" surface (PES) within the space of all possible nuclear configurations corresponding to the energetically easiest passage from reactants to products constrained to the Born–Oppenheimer approximation. In this sense, TS structure posses (locally) the highest potential energy among all possible chemical structures in that path at the expense of a minimum kinetic energy. Since the transition state theory [3, 4] is essentially based on the assumption that atomic nuclei behave according to classic mechanics, the presumption for the TS being represented by a chemical structure with a minimum kinetic energy which corresponds with a highly localized momentum density (locally) seems justified. Simultaneously, the TS will require a highly delocalized density in position space for the uncertainty principle to be satisfied. In this sense the Shannon entropies, as logarithmic descriptors of the electron density distributions in the combined phase space (normalized to unity), would correspond to extrema on the entropy profile at the vicinity of the TS, provided that the densities are adequately well represented in the chemical space.

The MEP represents the molecular potential energy of a proton at a particular location near a molecule [76], say at nucleus A. Then the electrostatic potential, V_A, is defined as

$$V_A = \left(\frac{\partial E^{\text{molecule}}}{\partial Z_A}\right)_{N, Z_{B \neq A}} = \sum_{B \neq A} \frac{Z_B}{|R_B - R_A|} - \int \frac{\rho(\mathbf{r})dr}{|\mathbf{r} - R_A|}, \tag{3}$$

where $\rho(\mathbf{r})$ is the molecular electron density and Z_A is the nuclear charge of atom A, located at R_A. Generally speaking, negative electrostatic potential corresponds to an attraction of the proton by the concentrated electron density in the molecules from lone pairs, pi-bonds, etc. (coloured in shades of red in standard contour diagrams). Positive electrostatic potential corresponds to repulsion of the proton by the atomic nuclei in regions where low electron density exists and the nuclear charge is incompletely shielded (coloured in shades of blue in standard contour diagrams).

We have also evaluated some reactivity parameters that may be useful to analyze the chemical reactivity of the processes. Parr and Pearson, proposed a quantitative definition of hardness (η) within conceptual DFT [77–78]:

$$\eta = \frac{1}{2S} = \frac{1}{2}\left(\frac{\partial \mu}{\partial N}\right)_{v(r)} \tag{4}$$

where $\mu = \left(\frac{\partial E}{\partial N}\right)_{v(r)}$ is the electronic chemical potential of an N electron system in the presence of an external potential $v(r)$, E is the total energy and "S" is called the softness within the context of DFT. Using finite difference approximation, Eq. 3 would be

$$\eta = \frac{1}{2S} \approx \frac{(E_{N+1} - 2E_N + E_{N-1})}{2} = \frac{(I - A)}{2} \tag{5}$$

where E_N, E_{N-1} and E_{N+1} are the energies of the neutral, cationic and anionic systems; and I and A, are the ionization potential (IP) and electron affinity (EA), respectively. Applying Koopmans' theorem [79–80], Eq. 4 can be written as:

$$\eta = \frac{1}{2S} \approx \frac{\varepsilon_{\text{LUMO}} - \varepsilon_{\text{HOMO}}}{2} \tag{6}$$

where ε denotes the frontier molecular orbital energies. In general terms, hardness and softness are good descriptors of chemical reactivity, the former measures the global stability of the molecule (larger values of η means less reactive molecules), whereas the S index quantifies the polarizability of the molecule [81–84], thus soft molecules are more polarizable and possess predisposition to acquire additional electronic charge [85]. The chemical hardness "η" is a central quantity for use in the study of reactivity and stability, through the hard and soft acids and bases principle [86–88]. However, in many cases, the experimental electron affinity is negative rather than positive, as such systems pose a fundamental problem; the anion is unstable with respect to electron loss and cannot be described by a standard DFT ground-state total energy calculation. To circumvent this limitation, Tozer and De Proft [89] have introduced an approximate method to compute this quantity, requiring only the calculation of the neutral and cationic systems which does not explicitly involve the electron affinity:

$$\eta = \frac{\varepsilon_{\text{LUMO}} - \varepsilon_{\text{HOMO}}}{2} + \varepsilon_{\text{HOMO}} + I \tag{7}$$

where I is obtained from total electronic energy calculations on the $N - 1$ and N electron systems at the neutral geometry $I = E_{N-1} - E_N$ and all energy quantities have to be calculated by continuum approximations, such as the local exchange–correlation functionals (GGA) to avoid integer discontinuities. Nevertheless, it has been observed that expression (7) does still work reasonably well with hybrids, such as B3LYP [89]. The authors have shown that this approximate method (Eq. 7) provided reasonable estimates for the electron affinities of systems possessing metastable anions, such as the case of CH_4 with large negative experimental electron affinity (-7.8 eV). We have employed Tozer and De Proft [90] approach for computing the hardness of the S_N2 ionic complex in order to test this approximation in a process departing from the ground-state requirement, such as the IRP of a chemical reaction. Atomic units are employed throughout the study except for the dipole moment (Debye) and the geometrical parameters (Angstroms).

3 Results and discussion

The electronic structure calculations performed in the present study were carried out with the Gaussian 03 suite of programs [91]. Reported TS geometrical parameters for the abstraction [92], and the S_N2 exchange reactions were employed [31]. Internal reaction coordinate (IRC) calculations [93] were performed at the MP2 (UMP2 for the abstraction reaction) level of theory with at least 35 points for each one of the reaction directions (forward/reverse) of the IRC path. Then, a high level of theory and a well-balanced basis set (diffuse and polarized orbitals) were chosen for determining all the properties for the chemical structures corresponding to the IRC path. Thus, the QCISD(T) method was employed in addition to the 6-311++G** basis set, unless otherwise be stated. The hardness and softness chemical parameters were calculated by use of Eqs. 6 and 7 and the standard hybrid B3LYP (UB3LYP for the abstraction reaction) functional [89]. Molecular frequencies corresponding to the normal modes of vibration depend on the roots of the eigenvalues of the Hessian (its matrix elements are associated with force constants) at the nuclei positions of the stationary points. We have found illustrative to calculate these values for the normal mode associated with the TS (possessing one

imaginary frequency or negative force constant) which were determined analytically for all points of the IRC path at the MP2 (UMP2 for the abstraction reaction) level of theory [91]. The molecular information entropies in position and momentum spaces for the IRC path were obtained by employing software developed in our laboratory along with 3D numerical integration routines [94, 95], and the DGRID suite of programs [96]. The bond breaking/forming regions along with electrophilic/nucleophilic atomic regions were calculated through the MEP by use of MOLDEN [97].

3.1 Radical abstraction reaction

The $H^. + H_2 \rightarrow H_2 + H^.$ is the simplest radical abstraction reaction involving a free radical (atomic hydrogen in this case) as a reactive intermediate. This kind of reaction involves at least two steps (S_N1 like): in the first step a new radical is created by homolysis and in the second one the new radical recombines with another radical species. Such homolytic bond cleavage occurs when the bond involved is not polar and there is no electrophile or nucleophile at hand to promote heterolytic patterns. When the bond is made, the product has a lower energy than the reactants and it follows that breaking the bond requires energy. Evidence will be presented elsewhere (Esquivel RO, Flores-Gallegos N, Iuga C, Carrera E, Angulo JC, Antolín J, unpublished) which shows that the two-step mechanism observed for this type of reaction is completely characterized by an asynchronous behavior but yet "concerted".

Our calculations for this reaction were performed at two different levels, the IRC was obtained at the UMP2/6-311G level and all properties at the IRC path were obtained at the QCISD(T)/6-311++G** level of theory. As a result of the IRC, 72 points evenly distributed between the forward and reverse directions of the reaction were obtained. A relative tolerance of 1.0×10^{-5} was set for the numerical integrations [94, 95].

In Fig. 1, the energy profile for the process is depicted, which shows the symmetric behavior of the IRC path. Also, in Fig. 1 we have depicted the entropy sum, which shows the exact opposite behavior as that of the energy, i.e., the TS represents a chemical structure with a localized density in the combined space of position and momentum (dual or phase space), which corresponds to a more delocalized position density with the lowest kinetic energy (more localized momentum density) among all the structures at the vicinity of the IRC path (see below). In this way the saddle point might be characterized by IT in the entropy hyper-surface.

The Shannon entropies in position and momentum spaces for the abstraction reaction are depicted in Fig. 2 in order to characterize its critical points at the IRC path by
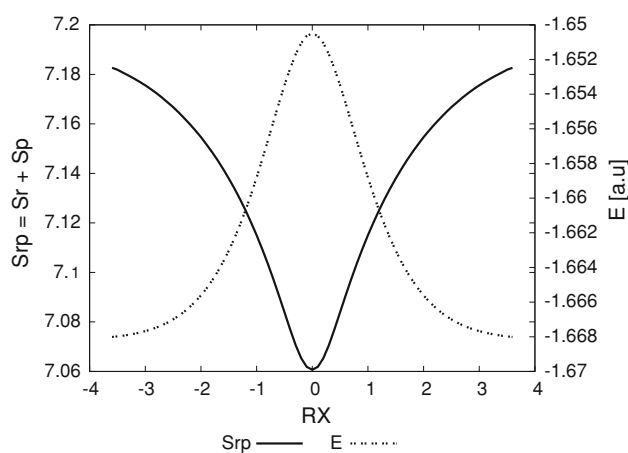

Fig. 1 Total energy values (*dashed line*) in a.u. and the entropy sum (*solid line*) for the IRC path of $H_a^. + H_2 \longrightarrow H_2 + H_b^.$
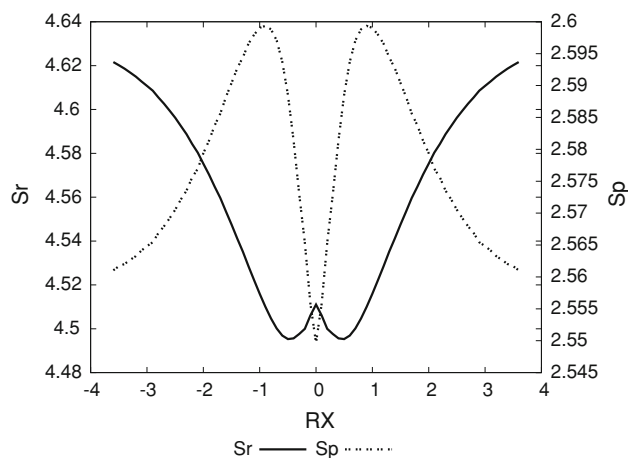

Fig. 2 Shannon entropies in position (*solid line*) and momentum (*dashed line*) spaces for the IRC path of $H_a^. + H_2 \longrightarrow H_2 + H_b^.$

use of several density descriptors discussed below. At first glance, we may note from Fig. 2 that the position entropy possesses a local maximum at the TS and two minima at its vicinity, whereas the momentum entropy possesses a minimum at the TS with two maxima at its vicinity, hence we observe that both quantities behave in opposite ways, i.e., the Shannon entropy in position space shows larger values toward the reactant/product complex ($H_a^. \cdots H-H_b$ and $H_a-H \cdots H_b^.$) and tends to decrease toward the TS region. In contrast, the momentum entropy increases as the intermediate radical ($H_a^.$) approaches the molecule, reaching maxima at the vicinity of the TS. This behavior is interpreted as follows: the position entropy values are smaller at the vicinity of the TS region as compared with the ones at the reactive complex region (toward reactants and products) since the densities of the chemical structures are globally more localized at the TS region (see Fig. 1 in connection with the entropy sum), which is the zone where

the important chemical changes take place. On the perspective of the momentum entropy, we may note that it is minimal at the TS which is linked to a more localized momentum density possessing the lowest kinetic energy value (maximum at the potential energy surface). At the reactive complex regions, momentum entropy values are larger than the TS one and therefore the corresponding kinetic energies are larger too, hence reproducing the typical potential energy surface shown in Fig. 1.

In Fig. 3, the bond distances between the entering/leaving hydrogen radicals and the central hydrogen atom are depicted. This clearly shows that in the vicinity of the TS a bond breaking/forming chemical situation is occurring since the R_{in} is elongating at the right side of the TS and the R_{out} is stretching at the left side of the TS. It is worth noting that the chemical process does not happen in a concerted manner, i.e., the homolytic bond breaking occurs first and then the molecule stabilizes by forming the TS structure which is clearly observed in the Fig. 3. As the incoming radical approaches the molecule the bond breaks, at the same location where the position entropy is minimum and the momentum entropy is maximum, then the TS is reached and the new molecule is formed afterwards. This is in agreement with the discussion above with regards to the two-step mechanism characterizing this reaction.

Next, we would like to test the non-polar bond pattern characteristic of homolytic bond-breaking reactions which should be reflected through the dipole moment of the molecules at the IRC path (note that the origin of the coordinate system is placed at the molecules's center of nuclear charge). This is indeed observed in Fig. 4, where these values along with the ones of the momentum entropy are depicted for comparison purposes. At the TS the dipole moment is zero, and the same is observed as the process
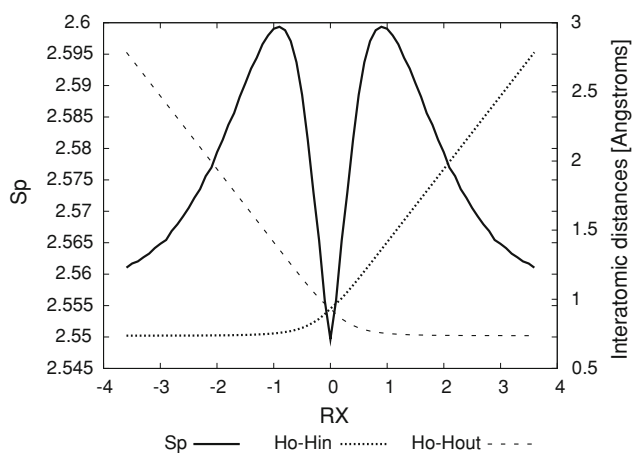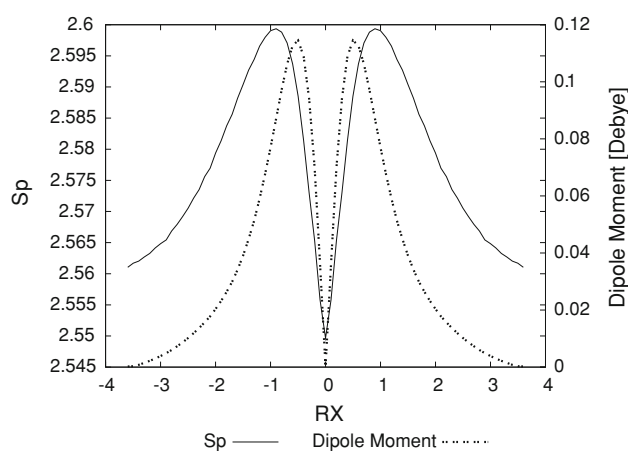

Fig. 4 Shannon entropy in momentum space (*solid line*) and the dipole moment values in Debye (*dashed line*) for the IRC path of $H_a^{\cdot} + H_2 \longrightarrow H_2 + H_b^{\cdot}$

tends to the reactants/products in the reaction path, reflecting the non-polar behavior of the molecule in these regions. However, it is also interesting to observe from this property, how the molecular densities get distorted, reaching maximal values at the vicinity of the TS, where the position entropies are minimal, i.e., at the bond-breaking/forming regions the complex exerts its largest distortion, where the position density is more localized. Once more, we may observe from Fig. 4 that the energy reservoirs for the bond cleavage occur earlier (or later depending on the direction of the reaction) at the IRC path as observed from the maxima of the momentum entropies. We will refer to these chemical regions as to bond cleavage energy reservoirs (BCER) in what follows.

In Fig. 5 the eigenvalues of the Hessian for the normal mode associated with the TS along the path of the reaction
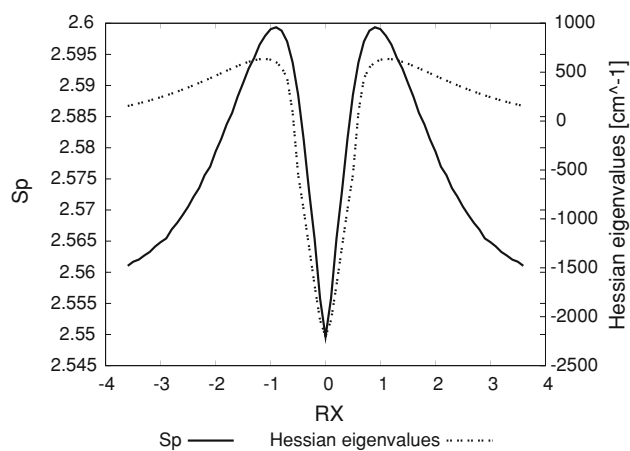

Fig. 3 Shannon entropy in momentum space (*solid line*) and the bond distances $R(H_0–H_{in})$ (*dashed line* for the entering hydrogen) and $R(H_0–H_{out})$ (*dotted line* for the leaving hydrogen) for the IRC path of $H_a^{\cdot} + H_2 \longrightarrow H_2 + H_b^{\cdot}$

Fig. 5 Shannon entropy in momentum space (*solid line*) and the eigenvalues of the Hessian (*dashed line*) for the IRC path of $H_a^{\cdot} + H_2 \longrightarrow H_2 + H_b^{\cdot}$. It should be noted that negative values actually correspond with imaginary numbers (roots of negative force constants) so that the negative sign only represents a flag

are depicted along with the momentum entropy values for comparison purposes. These Hessian values represent the transition vector "frequencies" which show maxima at the vicinity of the TS and a minimal value at the TS. Several features are worth mentioning, the TS corresponds indeed to a saddle point, maxima at the Hessian correspond to high kinetic energy values (largest "frequencies" for the energy cleavage reservoirs) since they fit with maximal values in the momentum entropy profile, and the Hessian is minimal at the TS, where the kinetic energy is the lowest (minimal molecular frequency) and it corresponds to a minimal momentum-entropy value. So it seems viable that the momentum entropy resembles the behavior of the TS vector.

The chemical reactivity behavior might be analyzed through density descriptors, such as the hardness and softness. In Fig. 6 we have plotted the values for the hardness along with the momentum space entropy for comparison purposes. From a DFT conceptual point of view we may interpret Fig. 6 as that chemical structures at the maximal hardness (minimal softness) values possess low polarizability and hence are less propense to acquire additional charge (less reactive). According to considerations discussed above, these structures are found at the BCER regions, i.e., they are maximally distorted, with highly localized position densities (minimal position entropies, see Fig. 2, and maximal dipole moment values, see Fig. 4). In contrast, hardness values are maximal at the reactant/product complex regions which correspond with delocalized position densities with null dipole moments, hence they are more prone to react (more reactive). At the TS, a local minimum for the hardness may be observed, then it is locally more reactive and leaning to acquire charge since its dipole moment is null. Accordingly, the TS structure is more relaxed and with a more delocalized density.

Since the results above might be affected by the effect of basis set we have performed a sensitivity analysis of the theoretic-information measures wherein 30 different basis sets were tested (presented elsewhere). We have observed that the qualitative structure of the entropies do not change significantly, which is shown in Fig. 7 where we present calculations at the MP2 level of theory for six different basis sets of the Pople [91] type to support the observations above.

3.2 Hydrogenic identity S_N2 exchange reaction

Continuing with our study we choose a typical nucleophilic substitution (S_N2) reaction since its chemical process involves only one step in contrast with the two-step S_N1 reaction. In the anionic form, the S_N2 mechanism can be depicted as $Y^- + RX \rightarrow RY + X^-$, which is characterized by being kinetically of second order (first order in each of
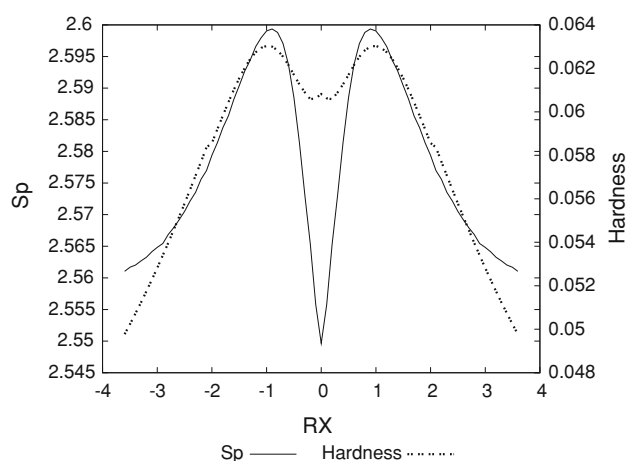

Fig. 6 Shannon entropy in momentum space (*solid line*) and the hardness values (*dashed line*) for the IRC path of $H_a^- + H_2 \longrightarrow H_2 + H_b^-$
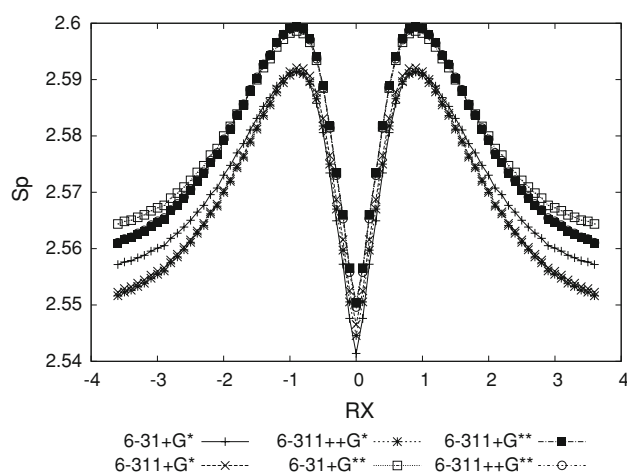

Fig. 7 Shannon entropies in momentum space for the IRC path of $H_a^- + H_2 \longrightarrow H_2 + H_b^-$ at the UMP2 level with increasingly larger bases: 6-31+G* (*vertical lines*), 6-311+G* (*crosses*), 6-311++G* (*stars*), 6-31+G** (*open squares*), 6-311+G** (*filled squares*) and 6-311++G** (*open circles*)

the reactants; the nucleophile Y^- and the substrate RX, where X^- is the nucleofuge or leaving atom). For identity S_N2 reactions $X = Y$. It was postulated that the observed second-order kinetics is the result of passage through the well-known Walden inversion transition state, where the nucleophile displaces the nucleofuge (leaving group) from the backside in a single-concerted reaction step. Evidence will be presented elsewhere (Esquivel RO, Flores-Gallegos N, Iuga C, Carrera E, Angulo JC, Antolín J, unpublished) which shows that the one-step mechanism observed for this type of reaction is indeed characterized by its synchronous and concerted behavior.

The $H_a^- + CH_4 \rightarrow CH_4 + H_b^-$ represents the typical identity S_N2 reaction and we proceed with the calculations

as follows: since diffuse functions are important to adequately represent anionic species [39], we have performed calculations for the IRC at the MP2/6-311++G** level of theory, which generated 93 points evenly distributed between the forward and reverse directions of the IRC. Then, all entropies and geometrical parameters at the IRC path were calculated at the QCISD(T)/6-311++G** level of theory which has been reported to be adequate for this kind of reactions [28]. A relative tolerance of 1.0×10^{-5} was set for the numerical integrations unless otherwise be stated [94, 95].

A comparison between the information entropies and the energy is shown in Fig. 8, wherein the entropy sum is depicted. The general observation is that both quantities behave in an opposite manner, although the entropy sum shows much more structure at the vicinity of the TS region as compared to the energy profile. It is important to mention that despite the entropy sum is very sensitive to changes in the densities (particularly the momentum density), as it may be observed from Fig. 8, we have verified through sensitivity analyses not reported here, that the entropy sum may be characterized by four different regions which are present beyond the inherent numerical instabilities of the integration algorithms or theoretical considerations, such as electron correlation or basis set effects. Hence, we distinguish three minima (one at the TS), two maxima and a significant change of curvature in between these critical points. Thus, toward the reactants/products we see larger values for the entropy sum (smaller energy values) which means that the corresponding complex ionic structures possess more delocalized structures in the joint space. At the TS we find the typical energy barrier (energy maximum) and a minimum for the entropy, which means that the TS structure is much more localized (in the joint space) than the reactant/product complex. Interestingly, two wider minima are found at the TS vicinity of the entropy sum at around $|R_X| \approx 1.5$–1.8 (at the forward/reverse side of the reaction), the origin of this zone will be analyzed below. Apparently, the chemical structures at these regions possess highly localized densities (in the combined space) as the TS structure does. Besides, two local maxima are found at the neighborhood of the TS, at around $|R_X| \approx 0.6$–0.7, which correspond to structures with more delocalized densities (in the joint space) as compared with the TS. Moreover, it is apparent from Fig. 8 that the entropy sum possesses more structure between the minima and maxima above described, at around $|R_X| \approx 0.9$–1.2, where a change of curvature is observed. The nature of the richer structure observed for the entropy sum (as compared with the energy), deserves to be explained and it will be revealed through the position and momentum entropies (depicted in Fig. 9), along with other
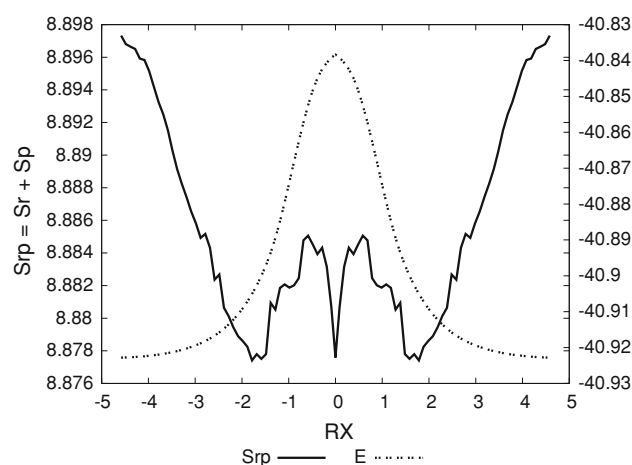

Fig. 8 Total energy values (*dashed line*) (a.u.) along with the Shannon entropy sum (*solid line*) for the IRC path of the S_N2 reaction
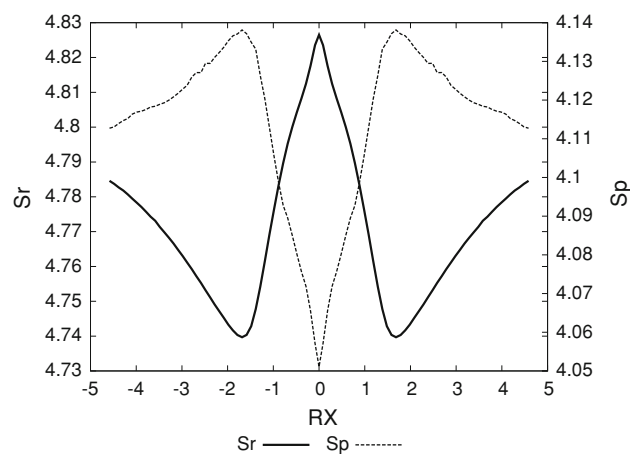

Fig. 9 Shannon entropies in position (*solid line*) and momentum (*dashed line*) spaces for the IRC path of the S_N2 reaction at the QCISD(T)/6-311++G** level

results for several descriptors of the densities presented below.

The Shannon entropies in position and momentum spaces for the exchange reaction have been analyzed elsewhere to describe the S_N2 reaction mechanism (Esquivel RO, Flores-Gallegos N, Iuga C, Carrera E, Angulo JC, Antolín J, unpublished). In this work, we have reproduced these measures in Fig. 9 in order to characterize the critical points at the reaction path by utilizing several density descriptors discussed below. From Fig. 9, we note that Shannon entropies in position and momentum spaces show a TS structure which is characterized by a delocalized position density and a localized momentum density, i.e., corresponding with a structurally relaxed structure with low kinetic energy. In contrast, as compared with the TS, the reactive complex toward reactants/products show more localized position densities with less

localized momentum densities, i.e., the chemical structures at these regions are structurally distorted and posses more kinetic energy as compared with the TS. At the vicinity of the TS, at around $|R_X| \approx 1.7$, critical points for both entropies are observed, minima/maxima for the position/momentum entropies, respectively. Thus, ionic complex at these regions characterize position densities which are highly localized and with highly delocalized momentum densities and high kinetic energies. At first glance, it seems likely that these regions correspond with BCER, where bond breaking may start occurring. It is interesting to note that BCER seem to be characterized by the entropy sum through the minima observed at the same region (see Fig. 8). Two more features that are worth noting is that both entropies show inflection points at $|R_X| \approx 1.0$ and maxima at $|R_X| \approx 0.5$, regions where the entropy sum shows more defined structure, change of curvature and maxima, respectively (see Fig. 8). We will come back later to these observations in connection with other properties.

To support our observations above we find instructive to plot the distances between the incoming hydrogen (H_a) and the leaving hydrogen (H_b) in Fig. 10. Distances show the stretching/elongating features associated with the bond forming/breaking situation that we have anticipated before. In contrast with the previous analyzed abstraction reaction, the S_N2 reaction occurs in a concerted manner, i.e., the bond breaking/forming starts taking place at the same time, in a gradual and more complicated manner as we explain below. An interesting feature which might be observed from Fig. 10 is that whereas the elongation of the carbon–nucleofuge (C–H_b) bond (R_b) changes its curvature significantly at $R_X \approx -1.7$ (forward direction of the reaction) the stretching of the nucleophile–carbon (H_a–C) bond (R_a) does it in a smooth way, posing the argument that bond breaking is occurring first, due to the repulsive forces that the ionic molecule exerts as the nucleophile approaches which provokes the breaking of the carbon–nucleofuge to happen as the molecule starts liberating its kinetic energy (decreasing of the momentum entropy). In this sense is that the reaction occurs in a concerted manner, i.e., the bond-breaking/dissipating-energy processes occurring simultaneously. At the near vicinity of the TS, around $R_X \approx -0.3$, we observe small changes for both interatomic distances revealed through minima in Fig. 10 (amplified picture), where it is apparent that repulsive forces occur at the TS. We will provide with more evidence of this effect below. Moreover, in Fig. 11 we have plotted the internal angle between H_a–C–H along with the Shannon entropy in position space for comparison purposes. Thus, the internal angle shows clearly that the molecule starts exerting the so called "inversion of configuration" at around $R_X \approx -1.7$, where the nucleophile starts displacing the nucleofuge
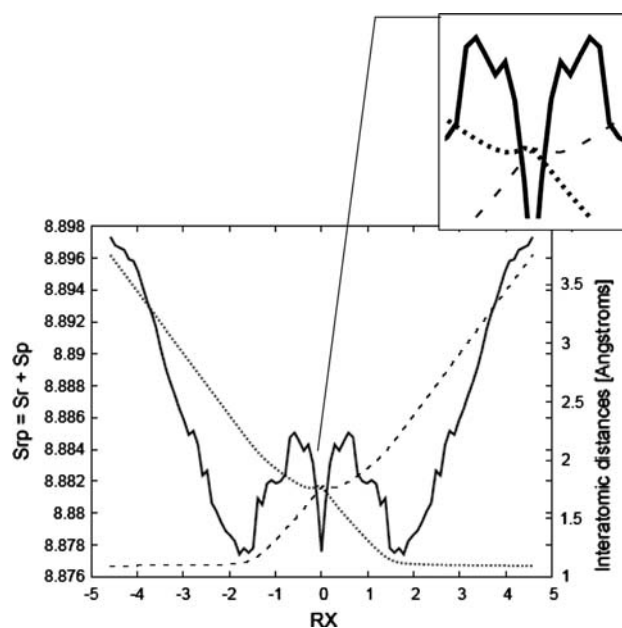

Fig. 10 Shannon entropy in momentum space (*solid line*) and the bond distance R_a (*dotted line*), corresponding to the H_a–C distance, and R_b (*dashed line*) corresponding to the (C–H_b) distance for the IRC path of the S_N2 reaction. In the side frame: detail of the minima observed for the bond distances at $R_X \approx -0.3$. Distances in Angstroms
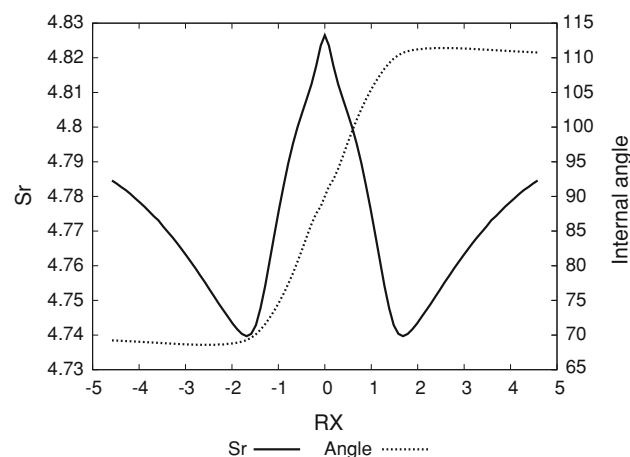

Fig. 11 Shannon entropy in position space (*solid line*) and the internal angle H_a–C–H (*dashed line*, where H_a stands for the nucleophile and H stands for any of the hydrogens attached to the methyl molecule for the IRC path of the S_N2 reaction. Angles in degrees

from the backside in a single concerted reaction step. This starts occurring at the BCER regions (see above).

The S_N2 reaction is an excellent probe to test the polar bond pattern characteristic of heterolytic bond-breaking (with residual ionic attraction because of the ionic nature of the products) which should be reflected through the dipole moment of the molecules at the IRC path (note that the
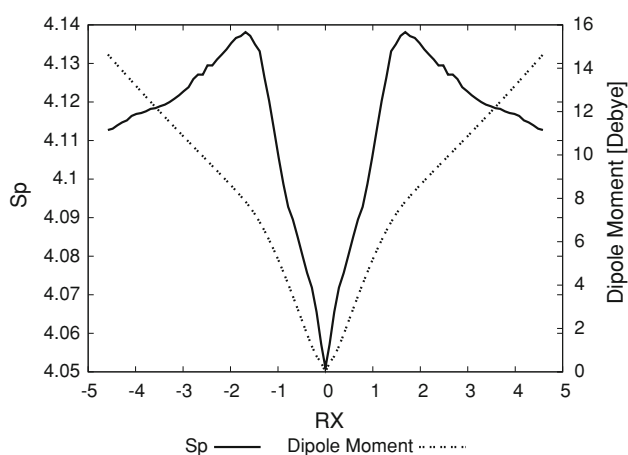
Fig. 12 Shannon entropy in position space (*solid line*) and the total dipole moment (*dotted line*) for the IRC path of the S_N2 reaction. Dipole moment in Debye

Fig. 13 Shannon entropy in momentum space (*solid line*) and the hardness values (*dashed line*) for the IRC path of the S_N2 reaction. Hardness in a.u

origin of the coordinate system is placed at the molecules's center of nuclear charge). This is indeed observed in Fig. 12, where these values along with the momentum entropy values are depicted for comparison purposes. At the TS the dipole moment is zero showing the non-polar character of the TS structure with both nucleophile/nucleofuge atoms repelling each other evenly through its carbon bonding. At this point the momentum/position entropies are minimal/maximal reflecting the low kinetic energy feature of the chemically relaxed TS structure. As the reactive complex approach the reactants/products region the dipole moment increases monotonically reflecting the polar bonding character of the ionic complex with a significant change of curvature at the TS vicinity at around $|R_X| \approx 1.0$ (a change of curvature was already noted for all entropies at the same region). In going from reactants to products it is evident that the inversion of the dipole moment values reflects clearly the inversion of configuration of the molecule (this reaction starts with a tetrahedral sp^3 carbon in the methyl molecule passing through a trigonal bipyramid structure and ends with a tetrahedral sp^3 in the product), which is an inherent feature of S_N2 reactions. It is also interesting to observe from the depicted property, how the molecular densities get distorted, reaching its largest deformation at the reactant/product regions, where the momentum/position entropies are larger/smaller than the TS, reflecting more tense structures with higher kinetic energies. Furthermore, we may observe from Fig. 12 that the BCER occur earlier in the forward direction of the reaction (at around $R_X \approx -1.7$) than the more acute deformation of the complex occurring at around $R_X \approx -1.0$. This may be simply interpreted at the light of the observations above in terms of the onset in which bond breaking occur. As the nucleophile approaches the molecule kinetic energy is collected so as to fill the BCER due
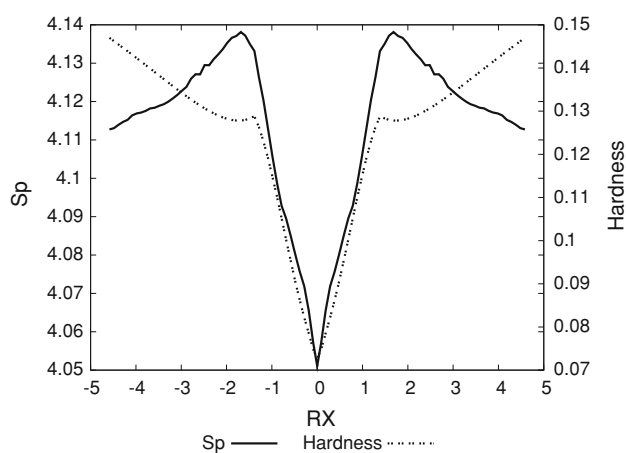
to the "collision" caused by the electrostatic repulsions of the nucleophile and the methyl molecule at $R_X \approx -1.7$. Next, as the reaction progresses, the accumulated energy at the BCER provide with the power for breaking the carbon–nucleofuge bond. In this manner, by utilizing observations of Figs. 10 and 11, we come across with an explanation for the change of curvature at around $R_X \approx -1.0$ (in the forward direction) observed for all entropies in that it is due to a bond-breaking process.

To provide with more evidence of the bond breaking region at around $R_X \approx -1.0$ we found illustrative to include the hardness values of the IRC path in the analysis, which is depicted in Fig. 13. It is interesting to observe from it the similarities between the hardness behavior and the one for the dipole moments of the reaction path in that both show largest values toward the reactant/product regions and minima at the TS, except for the observation that hardness possesses minima at the BCER regions. The interesting feature that we may comment from Fig. 13 is that the TS seems to be associated with a highly unstable structure since it has the lowest hardness (largest softness), i.e., the TS structure is highly polarizable as compared with the chemical species in the reaction path. Also, it may be observed from Fig. 13 that the reactive complex toward the reactant/product regions possess the largest hardness (lowest softness), which corresponds to highly stable molecules. Also interesting is to associate chemical significance to the BCER regions which show "hardness basins" that we interpret as to chemically metastable regions, energetically reactive and structurally stable, judging by the corresponding informational interpretation of the BCER discussed above. As the reaction progresses (in the forward direction) the hardness suddenly drops, falling into a well, where the energy is liberated to break the bond and, thus, forming a chemically reactive molecule
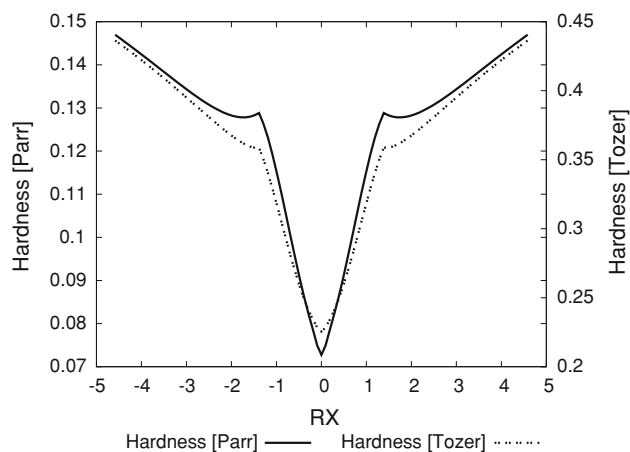
Fig. 14 Comparison of the hardness values obtained from Parr–Pearson Eq. 6 (*solid line*) and Tozer-De Proft Eq. 7 (*dotted line*) in a.u. at the B3LYP level of theory for the IRC path of the S_N2 reaction
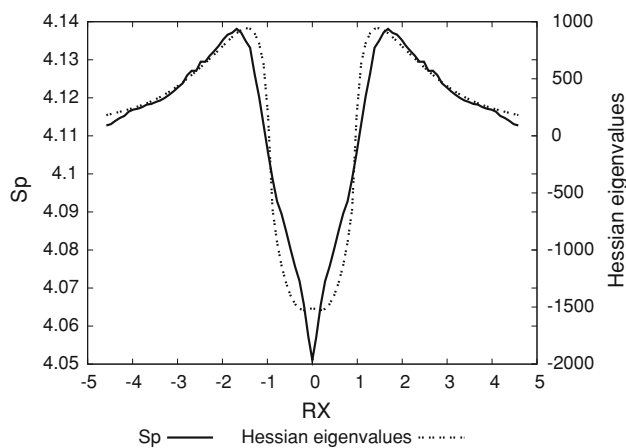

Fig. 15 Shannon entropy in momentum space (*solid line*) and the Hessian eigenvalues (*dashed line*) in a.u. for the IRC path of the S_N2 reaction. It should be noted that negative values actually correspond with imaginary numbers (roots of negative force constants) so that the negative sign only represents a flag

(highly polarizable structure) at the TS. So that, hardness is able to detect the BCER regions as well as the TS.

We have found interesting to use the S_N2 reaction as a probe for computing the hardness of the ionic complex at the reaction path of the S_N2 reaction in order to test Tozer and De Proft approximation [89] in a process departing from the ground-state requirement of DFT. In Fig. 14, a comparison of the hardness values obtained with Eqs. (6) and (7) are shown, which indicate that whereas the qualitative features are maintained, the numerical values change significantly. We may note also that the chemically metastable regions associated with the BCER mentioned above decay more rapidly into the TS well. A more elaborated study of the Tozer and De Proft approximation has been initiated in our laboratory in order to analyze the effects of several GGA functionals along with different bases (this will be presented elsewhere).

The eigenvalues of the Hessian for the normal mode associated with the TS along the IRC path are depicted in Fig. 15 along with the momentum entropy values, which are shown for comparison purposes. As it may be observed from Fig. 15, the Hessian values show maxima at the BCER and reach their minimal value at the TS. The former might be associated with high kinetic energy values (high vibrational frequencies) as compared to maximal values in the momentum entropy profile. The TS at the saddle point is associated with a low kinetic energy structure at the minimal molecular frequency value of the Hessian profile. It is interesting to note the resemblance between the momentum entropy profile and that of the TS vector.

To further support the above mentioned observations we can witness the physical process of bond breaking/forming through the contour values of the MEP at several stages of the S_N2 reaction in the plane of the H_a–C–H_b atoms which are depicted in Figs. 16 through 19. We may observe from

Fig. 16 the initial step of the bond breaking process for the leaving hydrogen H_b at $R_X \approx -1.5$ (forward direction), by noting that this particular atom is losing bonding charge (developing positive MEP and hence gaining electrophilic power) as it leaves. This is in contrast with the entering hydrogen which possesses the nucleophilic power of an hydride ion (enclosed by negative MEP).

It is also interesting to note that the remaining attached hydrogen atoms (shown in Figs. 16, 17, 18, 19 on the left side of the plane) possess the expected electrophilic nature (enclosed by positive MEP) of the molecular bonding environment although its "philic" nature barely change. In Fig. 17, at $R_X \approx -0.9$ in the forward direction of the reaction, the C–H_b bond cleavage has finished as the H_b atom loses bonding power (enclosed entirely by positive MEP/maximum electrophilic power), whereas the nucleophilic hydrogen H_a (enclosed by negative MEP) is about to form a new bond by losing charge (developing positive MEP/electrophilic power).

Then, the necessary charge transfer between the nucleophilic atom H_a and the leaving hydrogen H_b starts occurring at $R_X \approx -0.6$ in Figs. 18 and 19 (forward direction) as the former develops positive MEP (gaining electrophilic power) and the nucleofuge forms negative MEP (gaining nucleophilic power). At this reaction stage it is readily apparent that the molecular bond forming process has already started.

Figure 19 shows the repulsive effect we mentioned before in connection with the interatomic distances (Fig. 10) by noting that the leaving atom H_b is gaining nucleophilic power (negative MEP). The TS state which is not depicted shows a half and half electrophilic/nucleophilic character among the atoms, where the charge is evenly distributed throughout the molecule.
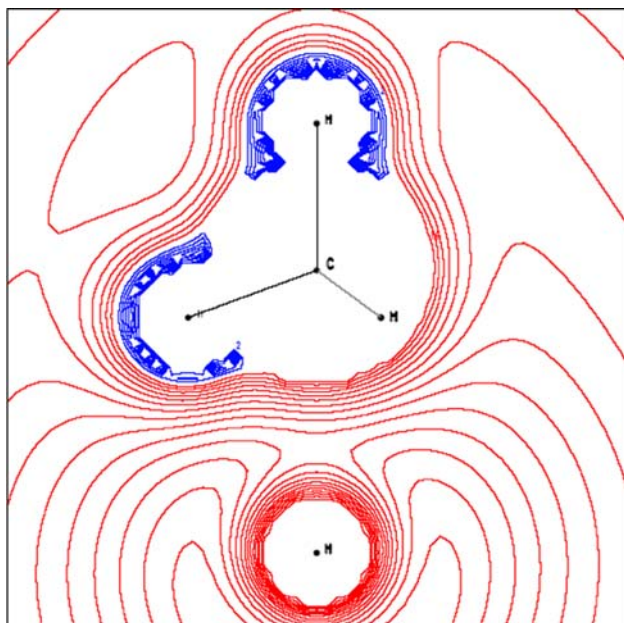
Fig. 16 The MEP contour lines in the plane of H_a–C–H_b (H_a stands for the nucleophilic atom and H_b is the nucleofuge, on bottom and top, respectively) showing positive MEP (nucleophilic regions) and negative MEP (electrophilic regions) at $R_X \approx -1.5$ for the S_N2 reaction
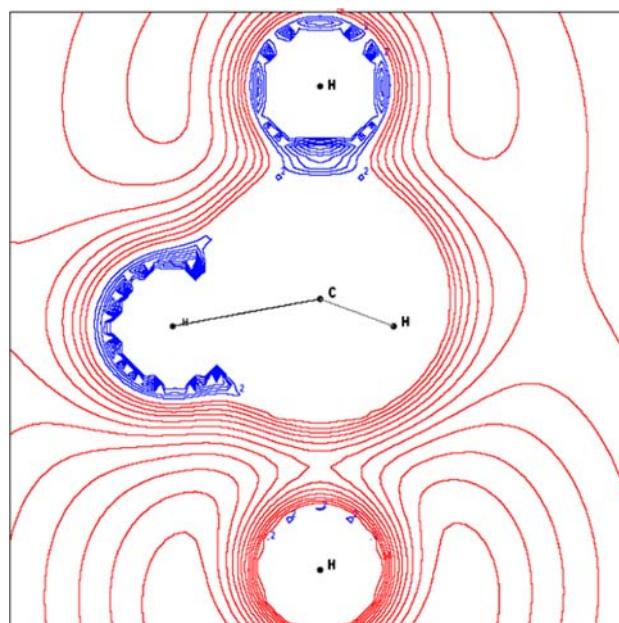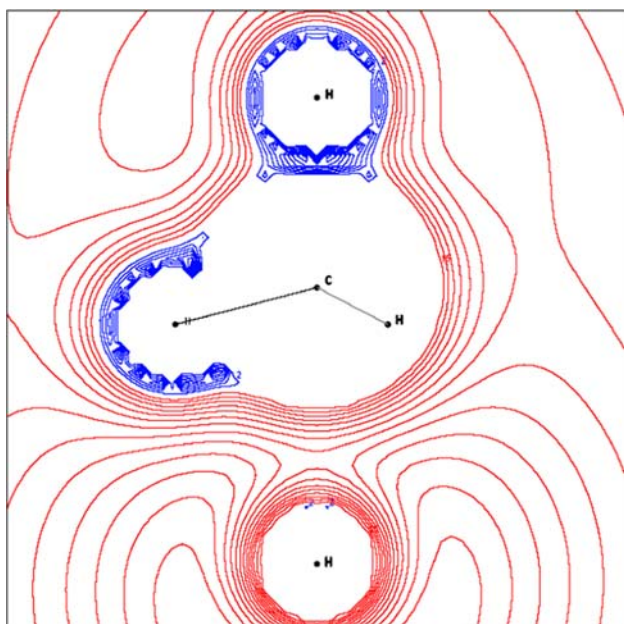

Fig. 18 The MEP contour lines in the plane of H_a–C–H_b (H_a stands for the nucleophilic atom and H_b is the nucleofuge, on *bottom* and *top*, respectively) showing positive MEP (nucleophilic regions) and negative MEP (electrophilic regions) at $R_X \approx -0.6$ for the S_N2
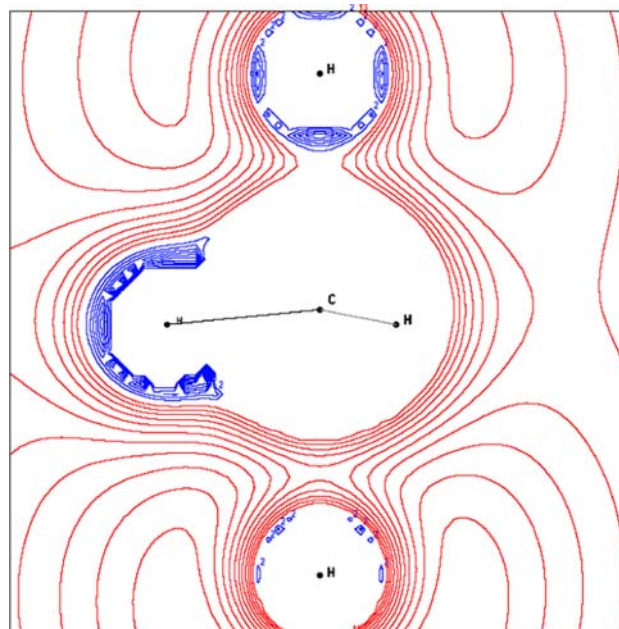

Fig. 17 The MEP contour lines in the plane of H_a–C–H_b (H_a stands for the nucleophilic atom and H_b is the nucleofuge, on *bottom* and *top*, respectively) showing positive MEP (nucleophilic regions) and negative MEP (electrophilic regions) at $R_X \approx -0.9$ for the S_N2 reaction

Fig. 19 The MEP contour lines in the plane of H_a–C–H_b (H_a stands for the nucleophilic atom and H_b is the nucleofuge, on *bottom* and *top*, respectively) showing positive MEP (nucleophilic regions) and negative MEP (electrophilic regions) at $R_X \approx -0.3$ for the S_N2 reaction

Therefore, according to the evidence we have presented we may summarize the process in the following manner: as the nucleophile approaches the molecule, repulsive forces

between the incoming and leaving hydrogens start to accumulate energy into the BCER regions, then the energy is dissipated through the bond-breaking process of the

leaving hydrogen, up to a point where the bond breaks and the incoming hydrogen (nucleophile) starts transferring charge and hence forming a new bond at the onset of the TS region. At the near vicinity of the TS a repulsive effect starts occurring between the nucleophile/nucleofuge atoms. The final remark is that all of the above observed phenomena are revealed by the Shannon entropies, note in particular the structure of the entropy sum which might be completely associated with the chemical phenomena occurring in the chemical reactions.

4 Conclusions

Throughout this study we have been able to assess the utility for the theoretic-information measures of the Shannon type to characterize elementary chemical reactions. The TS region of both the chemical reactions was detected and a plausibility argument of the connection between the TS and the Shannon entropies was provided and verified numerically. Besides, through these chemical probes we were capable to observe the basic chemical phenomena of the bond breaking/forming showing that the Shannon measures are highly sensitive in detecting these chemical events. It is worth mentioning that the results of the present study have also served the purpose of providing with evidence for the phenomenological mechanistic description of both reactions by revealing its synchronous/asynchronous behavior (Esquivel RO, Flores-Gallegos N, Iuga C, Carrera E, Angulo JC, Antolín J, unpublished).

Furthermore, the transition state of a reaction is commonly identified by the presence of a negative force constant for one normal vibrational mode corresponding with an imaginary frequency. However, the work of Zewail and Polanyi [36, 37, 98] in transition state spectroscopy has led to the concept of a reaction having a continuum of transient, a transition region rather than a single transition state. It is worth mentioning that the results of the present study show indeed the existence of such a region between the BCER before and after the TS. This is in agreement with reaction force, $\mathbf{F}(\mathbf{R})$, studies [47–50], where the reaction force constant, $\kappa(\mathbf{R})$, also reflects this continuum, showing it to be bounded by the minimum and the maximum of $\mathbf{F}(\mathbf{R})$, at which $\kappa(\mathbf{R}) = 0$.

This investigation suggests that more theoretic-information measures might be tested in order to perform a comprehensive study of the different options. It is well known that the Shannon entropy measure is of a global nature, whereas the so called Fisher information is of a local nature [99]. This is relevant in the context of chemical reactivity. Further, statistical complexity measures have been recently employed with success in analyzing diverse physical properties and processes [100–105], none of this

has been tested in the context of chemical reactivity. Also, it will be important for modern chemical reactivity to incorporate the effects of quantum correlations (entanglement) of the chemical species intervening in the chemical process [106–109]. Investigations along the above-mentioned lines have been initiated in our laboratories. This type of research might be useful for people in the quest of developing a complementary conceptual theory of the chemical reactivity along the lines suggested many times by Shaik et al. [110]. The more chemically meaningful information we can access about chemical processes, the more reliable and accurate the theories.

References

1. Hoffman R, Shaik S, Hiberty PC (2003) Acc Chem Res 36:750–756
2. Schlegel HB (1987) Adv Chem Phys 67:249–286
3. Eyring H (1935) J Chem Phys 3:107–115
4. Wigner E (1938) Trans Faraday SOC 34:29–41
5. Fukui K (1981) Acc Chem Res 14:363–368
6. González C, Schlegel HB (1990) J Phys Chem 94:5523–5527
7. Peng Ch, Schlegel HB (1993) Isr J Chem 33:449–454
8. Peng Ch, Ayala PhY, Schlegel HB, Frisch MJ (1996) J Comp Chem 17:49–56
9. Fan L, Ziegler T (1992) J Am Chem Soc 114:10890–10897
10. Safi B, Choho K, Geerlings P (2001) J Phys Chem A 105:591–601
11. Pople J, Krishnan AR, Schlegel HB, Binkley JS (1978) Int J Quantum Chem 14:545–560
12. González-García N, Pu J, González-Lafont A, Lluch JM, Truhlar DG (2006) J Chem Theory Comput 2:895–904
13. Ishida K, Morokuma K, Komornicki A (1977) J Chem Phys 66:2153–2156
14. Schmidt MW, Gordon MS, Dupuis M (1985) J Am Chem Soc 107:2585–2589
15. Baskin CP, Bender CF, Bauschlicher CW Jr, Schaefer HF III (1974) J Am Chem Soc 96:2709–2713
16. Shaik S, Ioffe A, Reddy AC, Pross A (1994) J Am Chem Soc 116:213–262
17. Hammond GS (1955) J Am Chem Soc 77:334–338
18. Leffler JE (1953) Science 117:340–341
19. Shaik S (1981) J Am Chem Soc 103:3692–3701
20. McWeeny R (1989) Methods of molecular quantum mechanics. Academic Press, London

21. Shaik S (1998) In: Schleyer PVR (ed) Encyclopedia of computational chemistry, vol 5. Wiley, Chichester, UK, pp 3143–3156
22. Shaik SS (1985) Prog Phys Org Chem 15:197–337
23. Shaik SS (1990) Acta Chem Scand 44:205–221
24. Shaik SS, Hiberty PC (1995) Adv Quantum Chem 26:99–163
25. Shaik SS, Shurki S (1999) Angew Chem Int Ed Engl 38:586–625
26. Shaik SS, Ch Reddy (1994) J Chem Soc Faraday Trans 90:1631–1642
27. Shaik SS (1988) J Am Chem Soc 110:1127–1131
28. Glukhovtsev MN, Pross A, Radom L (1995) J Am Chem Soc 117:2024–2032
29. Glukhovtsev MN, Pross A, Radom L (1996) J Am Chem Soc 118:6273–6284
30. Wolfe S, Mitchell DJ, Schlegel HB (1981) J Am Chem Soc 103:7692
31. Shi Z, Boyd RJ (1989) J Am Chem Soc 111:1575–1579
32. Pross A, Shaik S (1982) Tetrahedron Lett 23:5467–5470
33. Shaik S, Ioffe A, Reddy AC, Pross A (1994) J Am Chem Soc 116:262–273
34. Shaik SS, Ch Reddy (1994) J Chem Soc Faraday Trans 90:1631–1642
35. Shurki A, Shaik SS (1998) J Mol Struct (Theochem) 424:37–45
36. Zewail AH (1988) Science 242:1645–1653
37. Zewail AH (2000) J Phys Chem A 104:5660–5694
38. Bradforth SE, Arnold DW, Newmark DM, Manolopoulos DE (1993) J Chem Phys 99:6345–6359
39. Shi Z, Boyd RJ (1991) J Am Chem Soc 113:1072–1076
40. Bader RFW, MacDougall PJ (1985) J Am Chem Soc 107:6788–6795
41. Balakrishnan N, Sathyamurthy N (1989) Chem Phys Lett 164:267–269
42. Ho M, Schmider, Weaver DF, Smith VH Jr, Sagar RP, Esquivel RO (2000) Int J Quant Chem 77:376–382
43. Knoerr EH, Eberhart ME (2001) J Phys Chem A 105:880–884
44. Shaik SS, Schlegel HB, Wolfe S (1992) Theoretical aspects of physical organic chemistry: the S_N2 reaction. Wiley, New York
45. Tachibana AJ (2001) Chem Phys 115:3497–3518
46. Coulson CA (1961) Valence, 2nd edn. Clarendon, Oxford
47. Toro-Labbé A, Gutiérrez-Oliva S, Murray JS, Politzer P (2009) J Mol Model 15:707–710
48. Toro-Labbé A, Gutiérrez-Oliva S, Murray JS, Politzer P (2007) Mol Phys 105:2619–2625
49. Murray JS, Toro-Labbé A, Clark T, Politzer P (2009) J Mol Model 15:701–706
50. Jaque P, Toro-Labbé A, Geerlings P, De Proft F (2009) J Phys Chem A 113:332–344
51. Borgoo A, Jaque P, Toro-Labbé A, Van Alsenoy C, Geerlings P (2009) Phys Chem Chem Phys 11:476–482
52. Gadre SR (2003) In: Sen KD (ed) Reviews of modern quantum chemistry: a celebration of the contributions of Robert G. Parr, vol 1. World Scientific, Singapore, pp 108–147
53. Koga T, Morita M (1983) J Chem Phys 79:1933–1938
54. Ghosh SK, Berkowitz M, Parr RG (1984) Proc Natl Acad Sci USA 81:8028–8031
55. Angulo JC, Dehesa JS (1992) J Chem Phys 97:6485–6495
56. Antolín J, Zarzo A, Angulo JC (1993) Phys Rev A 48:4149–4155
57. Angulo JC (1994) Phys Rev A 50:311–313
58. Massen SE, Panos CP (1998) Phys Lett A 246:530–533
59. Ramirez JC, Perez JMH, Sagar RP, Esquivel RO, Ho M, Smith VH Jr (1998) Phys Rev A 58:3507–3515
60. Nalewajski RF, Parr RG (2001) J Phys Chem A 105:7391–7400
61. Nagy A (2003) J Chem Phys 119:9401–9405
62. Romera E, Dehesa JS (2004) J Chem Phys 120:8906–8912
63. Karafiloglou P, Panos CP (2004) Chem Phys Lett 389:400–404
64. Sen KD (2005) J Chem Phys 123:074110 (1–9)
65. Parr RG, Nalewajski RF, Ayers PW (2005) J Phys Chem A 109:3957–3959
66. Guevara NL, Sagar RP, Esquivel RO (2005) J Chem Phys 122:084101-1–084101-8
67. Shi Q, Kais S (2005) J Chem Phys 309:127–131
68. Chatzisavvas KC, Moustakidis CC, Panos CP (2005) J Chem Phys 123:174111–174300
69. Sen KD, Katriel JJ (2006) Chem Phys 125:074117 (1–4)
70. Nagy A (2006) Chem Phys Lett 425:154–156
71. Ayers W (2006) Theor Chem Acc 115:253–256
72. Martyusheva LM, Seleznev VD (2006) Phys Rep 426:1–45
73. Liu S (2007) J Chem Phys 126:191107 (1–3)
74. Shannon CE (1948) Bell Syst Tech J 27:379–423
75. Bialynicky-Birula I, Mycielski J (1975) Commun Math Phys 44:129–132
76. Politzer P, Truhlar DG (1981) Chemical applications of atomic and molecular electrostatic potentials. Academic Press, New York
77. Parr RG, Pearson RG (1983) J Am Chem Soc 105:7512–7516
78. Parr RG, Yang W (1989) Density-functional theory of atoms and molecules. Oxford University Press, New York
79. Koopmans TA (1933) Physica 1:104–113
80. Janak JF (1978) Phys Rev B 18:7165–7168
81. Ghanty TK, Ghosh SK (1993) J Phys Chem 97:4951–4953
82. Roy R, Chandra AK, Pal S (1994) J Phys Chem 98:10447–10450
83. Hati S, Datta D (1994) J Phys Chem 98:10451–10454
84. Simon-Manso Y, Fuenteaelba P (1998) J Phys Chem A 102:2029–2032
85. Chattaraj PK, Sarkar U, Roy DR (2006) Chem Rev 106:2065–2091
86. Pearson RG (1963) Hard and soft acids and bases. J Am Chem Soc 85:3533
87. Pearson RG (1973) Hard and soft acids and bases. Dowen, Hutchinson and Ross, Stroudsburg
88. Pearson RG (1997) Chemical hardness. Wiley–VCH, New York
89. Tozer DJ, De Proft F (2005) J Phys Chem A 109:8923
90. De Proft F, Chattaraj PK, Ayers PW, Torrent-Sucarrat M, Elango M, Subramanian V, Giri S, Geerlings P (2008) J Chem Theory Comput 4:595–602
91. Frisch MJ, Trucks GW, Schlegel HB, Scuseria GE, Robb MA, Cheeseman JR, Montgomery JA Jr, Vreven T, Kudin KN, Burant JC, Millam JM, Iyengar SS, Tomasi J, Barone V, Mennucci B, Cossi M, Scalmani G, Rega N, Petersson GA, Nakatsuji H, Hada M, Ehara M, Toyota K, Fukuda R, Hasegawa J, Ishida M, Nakajima T, Honda Y, Kitao O, Nakai H, Klene M, Li X, Knox JE, Hratchian HP, Cross JB, Bakken V, Adamo C, Jaramillo J, Gomperts R, Stratmann RE, Yazyev O, Austin AJ, Cammi R, Pomelli C, Ochterski JW, Ayala PY, Morokuma K, Voth GA, Salvador P, Dannenberg JJ, Zakrzewski VG, Dapprich S, Daniels AD, Strain MC, Farkas O, Malick DK, Rabuck AD, Raghavachari K, Foresman JB, Ortiz JV, Cui Q, Baboul AG, Clifford S, Cioslowski J, Stefanov BB, Liu G, Liashenko A, Piskorz P, Komaromi I, Martin RL, Fox DJ, Keith T, Al-Laham MA, Peng CY, Nanayakkara A, Challacombe M, Gill PMW, Johnson B, Chen W, Wong MW, Gonzalez C, Pople JA (2004) Gaussian 03, Revision D.01. Gaussian, Inc., Wallingford, CT
92. Johnson BA, Gonzales CA, Gill PMW, Pople JA (1994) Chem Phys Lett 221:l00–108
93. González C, Schlegel HB (1989) J Phys Chem 90:2154–2161
94. Pérez-Jordá JM, San-Fabián E (1993) Comput Phys Commun 77:46–56
95. Pérez-Jordá JM, Becke AD, San-Fabián E (1994) J Chem Phys 100:6520–6534

96. Kohout M (2007) Program DGRID, version 4.2
97. Schaftenaar G, Noordik JH (2000) MOLDEN: a pre- and post-processing program for molecular and electronic structures. J Comput Aided Mol Des 14:123–134
98. Polanyi JC, Zewail AH (1995) Acc Chem Res 28:119–132
99. Pennini P, Plastino A (2007) Phys Lett A 365:263–267
100. Sen KD, Antolín J, Angulo JC (2007) Phys Rev A 76:032502 (1–7)
101. Angulo JC, Antolín J, Sen KD (2008) Phys Lett A 372:670–674
102. Angulo JC, Antolín J (2008) J Chem Phys 128:164109 (1–7)
103. Montgomery HE Jr, Sen KD (2008) Phys Lett A 372:2271–2273
104. Szabó JB, Sen KD, Nagy Á (2008) Phys Lett A 372:2428–2430
105. Antolín J, Angulo JC (2009) Int J Quantum Chem 109:586–593
106. Huang Z, Kais S (2005) Chem Phys Lett 413:1–5
107. Huang S, Wang H, Kais S (2006) J Mod Opt 53:2543–2558
108. Flores-Gallegos N, Esquivel ROJ (2008) Mex Chem Soc 52: 19–30
109. Carrera E, Flores-Gallegos N, Esquivel RO (2009) J Comp Appl Math. doi:10.1016/j.cam.2009.02.086
110. Shaik SS (2007) New J Chem 31:2015–2028